Supporting Information

Thermoelectric Properties of PEDOT Nanowires/PEDOT Hybrids

Kun Zhang,[a] Jingjing Qiu[b], Shiren Wang[*a]

[a]Department of Industrial and Systems Engineering, Texas A&M University, College Station, TX 77843, USA

[b]Department of Mechanical Engineering, Texas Tech University, Lubbock, TX 79409-1021, USA

E-mail: s.wang@tamu.edu

1. Materials and Methods

1.1 Synthesis of PEDOT nanowires[1]

Sodium dodecyl sulfate (SDS, 30 mmol, Sigma-Aldrich, ≥99%) was dissolved in deionized (DI) water (100 ml). Subsequently, an aqueous solution of iron (III) chloride $FeCl_3$ (16.33 mmol, Sigma-Aldrich, ≥97%) was added to the SDS solution and stirred for 1 h at 50 °C. Then 3,4-ethylenedioxythiophene monomer (EDOT, 7 mmol, Sigma-Aldrich, 97%) was slowly added to the solution and the resultant solution was left on a hot plate to allow for polymerization for 6 h at 50 °C. After polymerization, the resultant PEDOT nanowire solution was purified with methanol and DI water for several times and then immediately re-dispersed in methanol with the aid of ultrasonication. In order to improve the dispersion of PEDOT nanowires, 5 vol% dimethyl sulfoxide (DMSO, Sigma-Aldrich, ≥99.5%) was added into PEDOT nanowire/methanol solution with another 15 min ultrasonication. The electrical conductivity of PEDOT nanowires film was measured to be ~450 S/cm.

1.2 Preparation of PEDOT NWs/PEDOT:PSS composite films

PEDOT:PSS (H. C. Starck) was filtered by a syringe filter (0.45 micron pore-size PVDF syringe filter) and mixed with 5 vol% DMSO for the subsequent process. 13.3 mg PEDOT nanowires (4 ml PEDOT nanowire/methanol/DMSO solution) was mixed with 10 ml PEDOT:PSS/5 vol% DMSO and subjected to 15 min ultrasonication. The thin film was prepared by spin-coating PEDOT nanowire/ PEDOT:PSS/5 vol% DMSO solutions at 4000 rpm for 40 seconds on a 13 mm ×13 mm glass substrate pre-cleaned with detergent, DI water, acetone and isopropanol in sequence. After spin-coating, the sample was thermally annealed at 130 ^{o}C for 15 min on a hot plate, and was subsequently immersed in ethylene glycol (EG, Sigma-Aldrich, anhydrous, 99.8%) solvent for a specific time at room temperature (50, 120, 220 and 300 min). After EG treatment, the sample was rinsed and washed in DI water to remove residual EG solvent. Finally, the treated sample was annealed on a hot plate at 120 ^{o}C for another 15 min.

1.3 Preparation of PEDOT NWs/PEDOT-Tos composite films

PEDOT-Tos thin films were prepared via a vapor-phase polymerization (VPP) method reported elsewhere. [2-3] In a typical procedure, 2 g Clevios™ C-B 40 V2 (40 wt% Iron (III) tosylate (Fe(Tos)$_3$) in n-butanol), 1.5 g PEG-PPG-PEG (M_w=5800, Sigma-Aldrich) and 1.5 g dimethylformamide (DMF, Sigma-Aldrich) and 1.5 g n-butanol were pre-mixed. The tripolymer PEG-PPG-PEG and DMF were used to control the crystallization of PEDOT. The mixture was ultrasonicated for 10 min to mix thoroughly. Microscope glass slides were cut into 13 mm by 13 mm and washed with detergent, DI water, acetone and isoproponal in sequence. These washing steps help the oxidant solution to wet the glass substrate. The vial with oxidant solution was placed on a hotplate at 35 ^{o}C for ~2 minutes prior to pipetting solution. Subsequently, the oxidant solution was dropped and

covered the entire glass substrate. Then the substrate was spin-coated at 1500 rpm for 25 sec and immediately transferred onto a hotplate at 70 °C for 30 sec. Finally, the substrate was transferred to a vacuum oven with a crucible having EDOT monomers at the bottom of the chamber. The vapor-phase polymerization was conducted in the chamber at 35 °C under a pressure of 45 mbar. After 25 min, the sample was removed from the chamber and placed on a hotplate at 70 °C for 2 min and then cooled down to room temperature. The resultant PEDOT-Tos thin film was thoroughly washed with ethanol to remove any oxidant residuals. The washed film was finally dried in air for further characterization. To fabricate PEDOT NW/PEDOT-Tos composite film, 0.2 wt% PEDOT NWs were added into the above oxidant solution with tip ultrasonication for 1 hour. Other steps are identical to that of the fabrication of PEDOT-Tos films.

2. Structure characterizations

The PEDOT nanowire structure was characterized by transmission electron microscope (TEM, Hitachi 8100, 75 kV, Figure 1), X-ray diffraction (XRD, Figure 1), and atomic force microscope (AFM, XE-100, contact mode with the scanning rate=1 Hz, Figure S1). The XRD patterns were collected with Powder X-Ray Diffraction (PXRD) with a Rigaku Ultima III diffractometer using Cu Kα radiation. To prepare the samples for X-ray powder diffraction, samples were finely ground. The measurements were taken at a 2θ range of 5-40° at a step-width of $0.03°$ sec^{-1}.
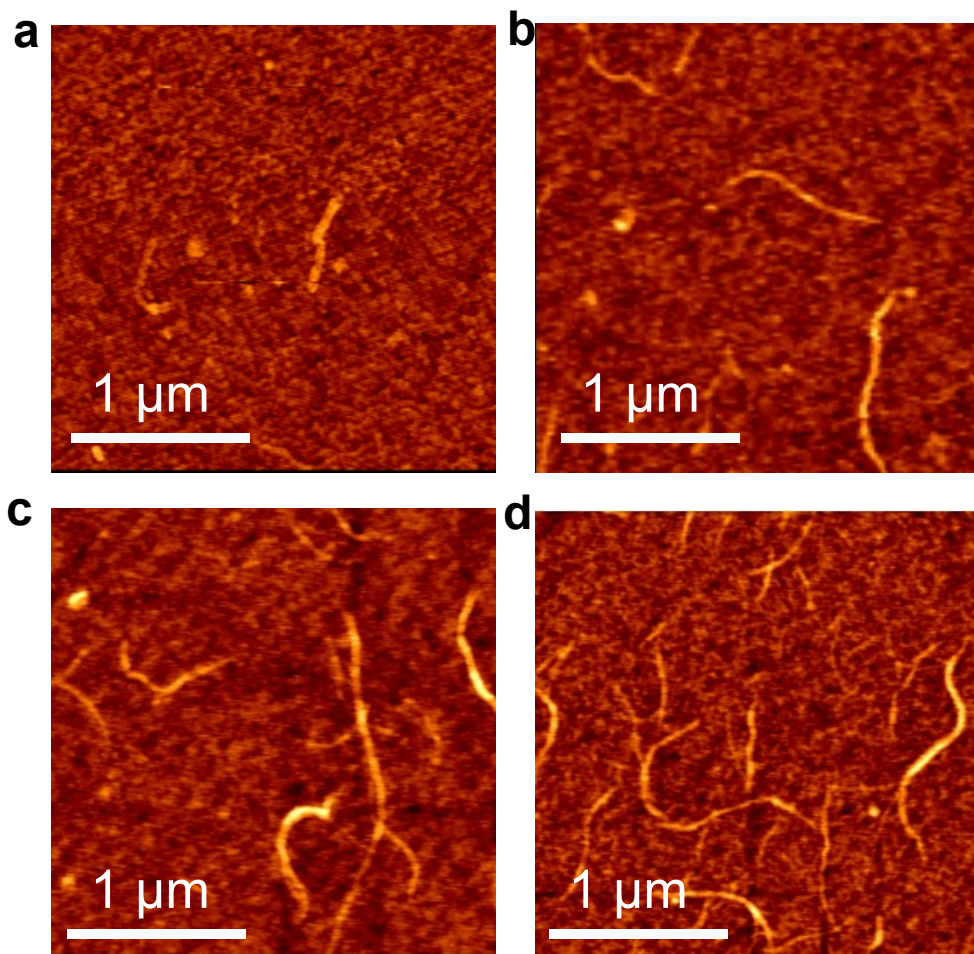
Figure S1. AFM topography images of PEDOT NWs/PEDOT:PSS hybrid films with various PEDOT NW weight fractions. a, 0.1 wt%. b, 0.2 wt%. c, 0.5wt%. d, 1 wt%. Samples with high NW fraction (0.5 and 1 wt%) hybrids show percolated networks.

3. Carrier mobility measurement by organic electrochemical transistors (OECTs)

We firstly made several trials with standard organic field-effect transistor (OFET) devices for the mobility measurement of highly doped PEDOT samples, however, no field effects were observed, which also has been reported in the literature.[7] In this work, the linear carrier mobility of PEDOT samples were evaluated with the side-gate OECTs as reported in the literature.[7-8] The side-gate OECT architecture is utilized because

PEDOT:PSS is highly doped with the carrier concentration typically more than 10^{20} cm^{-3}, which could screen the electric field in standard OFET devices.[7] In standard OFET architecture (i.e. bottom-gate bottom-contact), the carriers are accumulated at the interface between the active semiconductor layer and the dielectric layer by applying a electric field at the gate. But in PEDOT:PSS, carriers are always present due to its high doping level. For this reason applying a field doesn't have much effect as the existing free carriers simply respond to an externally applied field by moving towards the lowest energy level and therefore shield the material from the field. In some low doping levels of PEDOT:PSS there may still be a small field effect, but in highly doped PEDOT:PSS, such as PEDOT:PSS, there is unlikely to be any effect. Hence, this is the reason why we conducted the linear carrier mobility measurements with electrolyte-gated electrochemical transistors. Further evidence will be provided to explain the reliability of measuring linear mobility with OECT devices.

Here, a side-gate OECT architecture was used to measure the linear carrier mobility of highly doped PEDOT:PSS as reported in the literature.[7-8] Ion gel was used to introduce a higher density of charge carriers. As shown in Figure S2, transistors with a channel length (L) of 50 μm and width (W) of 6 mm were fabricated in a bottom-contact side-gate configuration on the SiO$_2$ substrates. Au was used for the source, drain, and gate electrodes. Ion gels based on poly(vinylidene fluoride-co-hexafluoropropylene) (P(VDFHFP)) and the ionic liquid 1-ethyl-3-methylimidazolium bis(trifluoromethylsulfonyl)amide ([EMI$^+$][TFSA$^-$]) were used as the dielectric layer. The thickness of PEDOT:PSS layer is 20–50 nm, and the thickness of ion gel dielectric layer is ~ 6 μm.
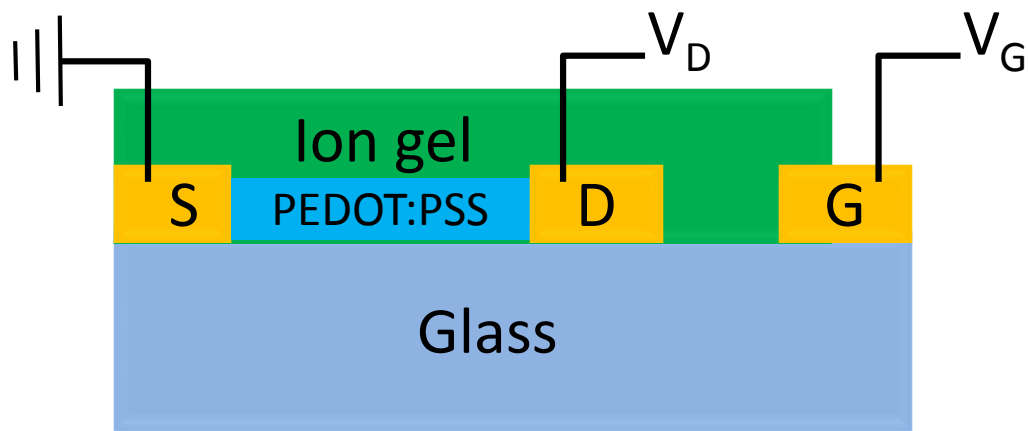
Figure S2. Illustration of side-gate OECT device for the linear carrier mobility measurement. S: Source electrode, D: Drain electrode, G: Gate electrode. V_D: Source-drain voltage, V_G: Gate voltage.

The active layer of OECT devices was formed by spin-coating with a uniform thin layer (<50 nm). Cotton swabs soaked in solvents (ethanol for PEDOT:PSS) were used to thoroughly wipe clean contact pads and the rest of the substrates with the exception of the area around the channel. A high precision cotton swab was used to clean between devices to avoid cross-talking and reduce leakage.

Two Keithley 2400 source-meters were used both to provide gate and drain voltages, and also as the drain-source current meter by connecting the gate and drain socket on the probe station to two Keithley 2400 using two shielded coaxial cables. In general the Keithley 2400 is used as a voltage source and current is measured on auto range with a compliance of ~1 mA. The linear mobility $\mu(lin)$ is calculated from the following equation:[7]

$$\mu(lin) = \frac{L}{W \bullet C_i} \frac{\partial g_d}{\partial V_G}$$

where C_i (=12 $\mu F/cm^2$ at 1 Hz) is the dielectric capacitance per unit area of the ion gel dielectric layer,[7] the capacitance will decrease as the measured frequency increases;[8,9] $g_d = I_D/V_D$ is the conductance, which was calculated using the linear regime (small drain voltage) of output curves when the gate voltage is small that the ions in ion gels haven't penetrated and dedoped the polymer channel, I_D is the source-drain current, V_D is the source-drain voltage, V_G is the gate voltage, L =50 μm and W=6 mm are the channel length and width. Figure S3 shows typical output characteristics and conductance of PEDOT-based OECT devices for linear mobility evaluation. (Note: Several same samples were measured for each type of OECT device.) Linear mobility results are shown in Table S1.

As shown in Figure S3a, clear field effect can be observed in all samples, which should be due to the de-doping of PEDOT samples as the gate voltage is high, which has been experimentally verified by Wei *et al* with the *in situ* UV–vis–NIR spectroscopy.[7] The electrochemical doping mechanism also has been extensively studied in poly(3-hexylthiophene) (P3HT) or other organic semiconductors-based electrolyte-gated OECT devices.[10-12]
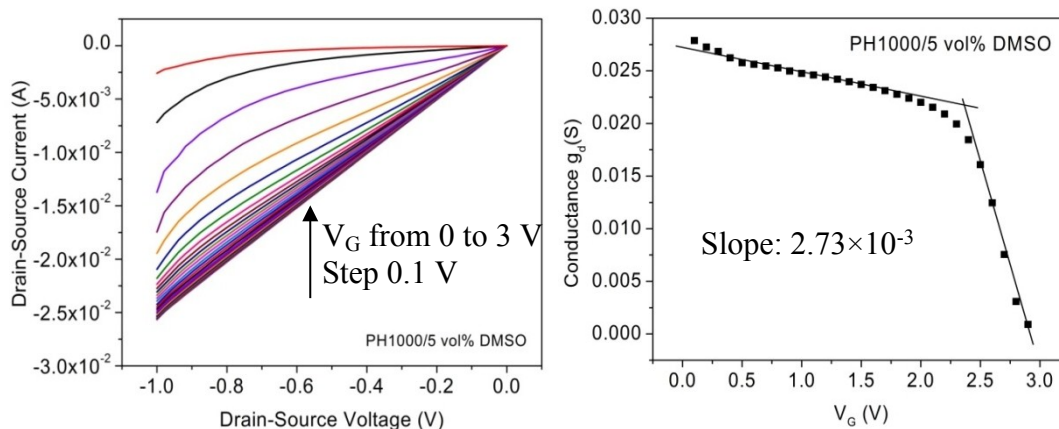
Figure S3. a, Output curves of the OECT using 5 vol% DMSO/PEDOT:PSS as the active channel. **b,** Conductance curves as a function of gate voltage for OECT using 5 vol% DMSO/PEDOT:PSS as the active channel.

As displayed in Figure S3b, the conductance was plotted as a function of gate voltage. As the gate voltage is low, the conductance g_d shows linear decrease as the positive gate voltage increases, which should be attributed to the linear decrease of carrier concentration in polymer channels. The carriers in this regime should comply with a two-dimensional transport at the interface between PEDOT channels and ion gels.[10,12]

As the gate voltage is large enough, the ions in ion gels can penetrate into PEDOT channels introducing the electrochemical de-doping of PEDOT samples. It is believed to follow with the three-dimensional charge transport, indicating the carriers are transported through the bulk of PEDOT materials.[10] As seen in Figure S3b, as the applied gate voltage increases, there are inflection points in all samples that the electrochemical de-doping of PEDOT samples resulted in dramatic decreasing of the conductance with a larger slope. It is worth to note that the diffusion of ions into the bulk of PEDOT channels depends not only on the gate voltage but also on the scanning rate of gate voltage. A long enough time at low gate voltage would also result in the diffusion of ions. So a proper

scan rate of gate voltage was used (0.1V/s). Moreover, it can be seen that there is no saturation regime for these PEDOT-based transistors, thus only the evaluation of linear carrier mobility in the linear regime is plausible. And based on the two-dimensional transport in this regime, the formula for the linear mobility calculation in organic field-effect transistors is valid in this work.

Table S1. Averaged linear carrier mobility results of PEDOT:PSS, PEDOT-Tos, PEDOT:PSS /5 vol% DMSO with various EG treatment times.

Samples	μ (cm2/Vs)
5 vol% DMSO/PEDOT:PSS, EG 0 min	**2.02±0.11**
5 vol% DMSO/PEDOT:PSS, EG 50 min	**2.41±0.26**
5 vol% DMSO/PEDOT:PSS, EG 120 min	**3.18±0.35**
5 vol% DMSO/PEDOT:PSS, EG 220 min	**3.51±0.18**
PEDOT:Tos	1.78±0.13

Note: For all EG treated PEDOT:PSS, 5 vol% DMSO was added before spin-coating.

4. Work function measurement

Work functions (WFs) of the polymer samples were measured with both x-ray photoelectron spectroscopy (XPS) and Kelvin probe, with the results using both methods showing good agreement. It was found by Kelvin probe (KP) method that PEDOT NW samples have a very similar work function except PEDOT NW with 220 min EG treatment, so we use a single average work function value for PEDOT NW with 0, 50, 120 and 300 min EG treatment. So the work function offsets between PEDOT:PSS and PEDOT NW were calculated based on the Kelvin probe method, see Table S2 for details.

Kelvin probe work function measurements were performed on an SKP SPV LE 450 Scanning Kelvin Probe Surface Photovoltage instrument from KP Technology. KP measurements were performed in air with a probe oscillation frequency of 78 kHz. The

XPS work function measurements were performed in ultrahigh vacuum on a PHI 5600 ESCA instrument, which has been discussed previously.[13] We note that the secondary electron cutoff region is photon energy independent. Thus, we calibrated the energy scale for the secondary electron cutoff region using ultraviolet photoelectron spectroscopy (UPS) with known metallic standards (Au, Mo, Cu, or Ag), which results in an uncertainty of +/- 0.025 eV for the extracted work function. The work function for each sample was determined by measuring the secondary-electron cut-off region. Specifically, we fit the baseline and secondary-electron cut-off to a line; the intercept of the two determines the work function (work function = 21.218 eV – intercept). Interestingly, in some samples, the secondary electron cutoff region has a small additional shoulder at higher binding energy. The origin of this shoulder is unclear, but may be due to a minority phase within the material. In all samples, we fit the secondary electron cutoff that represents the majority of the signal to ensure consistent comparisons for the sample work functions. Work functions were referenced to three different metallic samples – platinum, gold, and Inconel – that were stored in air and were not rigorously cleaned before XPS or KP measurements. The work functions of the reference samples were determined by XPS to be 5.13, 5.03, and 4.37 eV for platinum, gold, and Inconel, respectively. The work function of a given polymer sample was calculated from the linear regression fit to the standards, as shown in Figure S4.
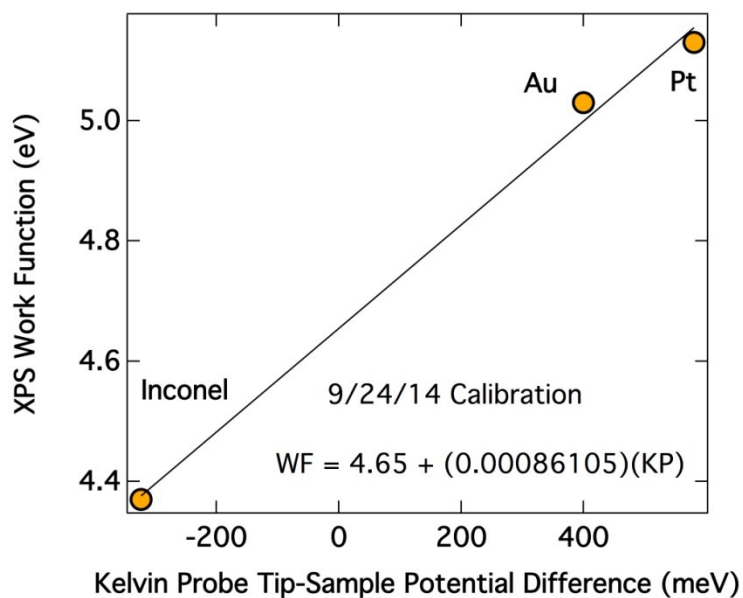
Figure S4. Calibration curve for Kelvin probe measurement, based on XPS-measured work function values for three reference samples: gold, platinum, and Inconel (gold data points). A given polymer sample's work function is calculated from the measured Kelvin probe potential difference (KP), using the equation determined by the linear regression fit shown as the solid line.

Table S2. Work functions of as-received PEDOT:PSS, PEDOT-Tos, 5 vol% DMSO/PEDOT:PSS with different EG treatment times.

EG treatment time (min)	WF of 5 vol% DMSO/PEDOT:PSS (eV)	WF of PEDOT NWs (eV)	Interfacial barrier ΔE (eV)
0	**4.88**	**4.78**	**0.10**
50	**4.92**	**4.78**	**0.14**
120	**4.87**	**4.78**	**0.09**
220	**4.85**	**4.78**	**0.07**
300	**4.82**	**4.78**	**0.04**
PEDOT:Tos	4.63	4.78	-0.15

5. Thermoelectric properties characterizations

5.1 The electrical conductivity measurement

The Van der Pauw method was employed for electrical conductivity measurements (Figure S5). Electrical contacts were made by thermally depositing gold electrodes (1.5 mm by 1.5 mm) on four corners of the thin film on glass substrate. I-V sweeps were performed using a Keithley 6221 current source and a Keithley 2182A nanovoltmeter. DC current was applied from corner 2 to corner 1, and the voltage was measured between corner 3 and corner 4, R_A was calculated as $(V_{3,4}/I_{1,2} + V_{1,2}/I_{3,4})/2$. DC current was applied from corner 3 to corner 2, and the voltage was measured between corner 1 and corner 4, R_B was calculated as $(V_{1,4}/I_{2,3} + V_{2,3}/I_{1,4})/2$. By measuring R_A and R_B, the electrical conductivity can be calculated by the following equation: [14]

$$\sigma = \left[\frac{\pi d}{\ln 2} \bullet \frac{(R_A + R_B)}{2} \bullet f(\frac{R_A}{R_B}) \right]^{-1}$$

,where d is the film thickness (measured by AFM, XE-100), $f(x)=1/cosh(ln(x)/2.403)$ is the correction factor.[14]
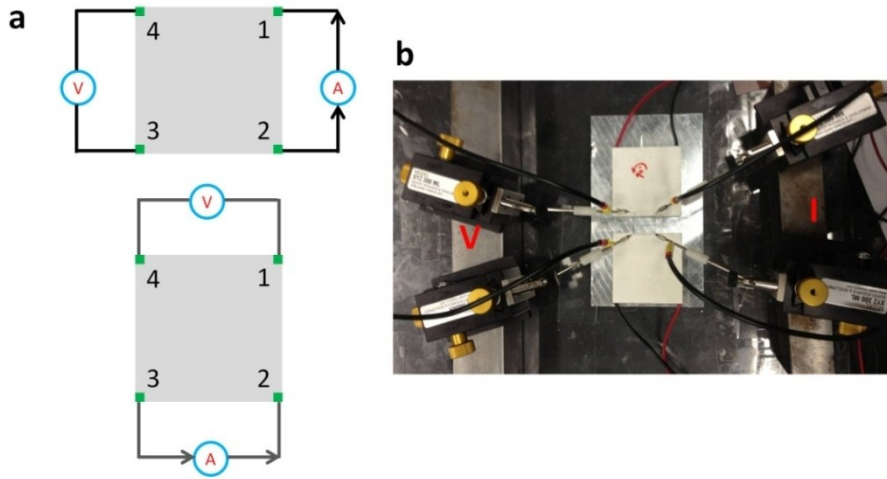
Figure S5. Illustrations of the Van der Pauw method for electrical conductivity measurements. **a,** Schematic diagram of the Van der Pauw method. **b,** Photo of the Van der Pauw measurement system.

5.2 The Seebeck coefficient measurement[15,16]

To determine the Seebeck coefficient of conducting thin films, a Peltier heater was used to heat one side of thin films, a Peltier cooler was used as the heat sink to cool another side of thin film (Figure S6). The relative humidity is ~17% during measurements. Prior to the measurement, a pair of square gold electrodes (1 mm × 7 mm × 150 nm) with the spacing l of 10 mm was thermally deposited on each film to define the electrical measurement spacing. Two T-type micro-thermocouples (TCs, diameter of 127 μm) were placed on the thin film to the left of the left electrode and to the right of the right electrode with a spacing of L, which is much larger than the TC diameter, and the error in TC position. Polymer in the region of the TCs was erased by a hard swab with ethanol in order to eliminate the interruption to the thermal voltage measurement. The measured temperature difference between TCs was defined as ΔT_{TC}, thus the actual temperature

difference between electrodes is $\Delta T = \Delta T_{TC} \times l/L$. Further experiments and simulation proved that the temperature profile along the direction of TCs is linear. To measure the Seebeck voltage ΔV, two gold micro-wires (diameter of 25 µm) were brought into contact with the gold electrodes with the assistance of indium. The Seebeck coefficient is thus defined as S= -$\Delta V/\Delta T$.
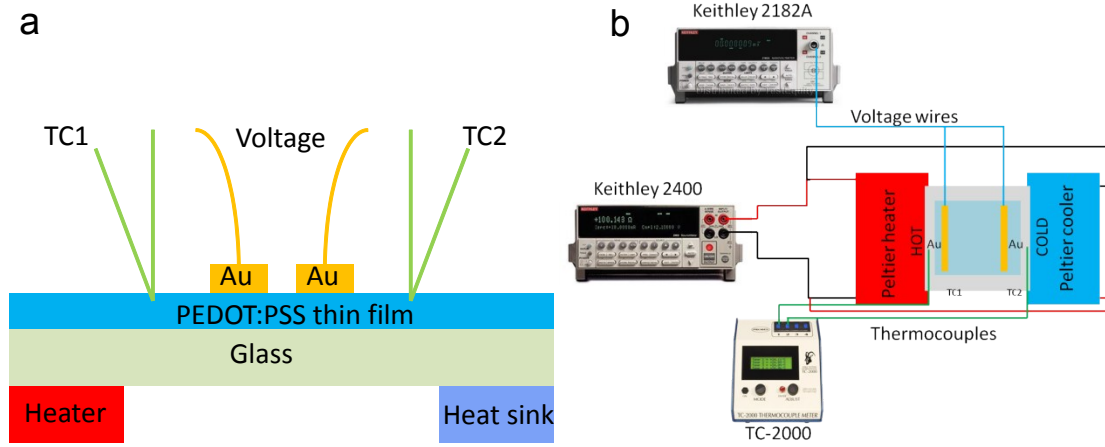

Figure S6. Illustrations of the Seebeck coefficient measurement. **a**, The side-view of the Seebeck coefficient measurement setup. **b**, The schematic diagram of the Seebeck coefficient measurement setup assembling.

Prior to the Seebeck coefficient measurement, the one-dimensional temperature distribution across the thin film surface was investigated. For a barrier with a constant thickness, the rate of heat loss is given by:

$$\frac{Q}{t} = \frac{\kappa A(T_{hot} - T_{cold})}{d}$$
$$\Rightarrow \frac{(T_{hot} - T_{cold})}{d} = \frac{Q}{t\kappa A}$$

,where Q is the heat flux, t is the unit time, κ is the thermal conductivity of thin film, T_{hot} is the hot side temperature, T_{cold} is the cold side temperature, A is the cross-sectional area of the thin film, and d is the distance between the hot side and the cold side.

For a direct current (DC) powered heat source (Peltier heater), the heat flux Q is constant for unit time. For a given sample, the thermal conductivity κ and the cross-sectional area A are also constant. Thus the temperature difference per unit length $(T_{hot} - T_{cold})/d$ is constant for the thin film. Hence the one-dimensional temperature distribution is linear from the hot side to the cold side.

To demonstrate this linear temperature distribution, temperatures of four selected points on the thin film were measured. As illustrated in the inset of Figure S7a, four T-type micro-thermocouples (TCs, diameter of 127 μm) were placed collinearly with various distances (which is much larger than the TC diameter and the error in TC position) between each other on the thin film. (Note: In order to avoid the effect of heater and cooler on the accuracy of the temperature measurements, TCs were placed away from the heater and cooler edges with a distance of > 2 mm.) When the temperature was stable, temperatures were collected and found to vary linearly with respect to the distance between the TC position (where the temperatures were measured) and the heater edge (Figure S7a). Temperatures with respect to the distance between the TC position and the heater edge were captured for 12 min and found to be linear at a specific time (Figure S7b). The same trend was found through the temperature simulation as seen in Figure S8.
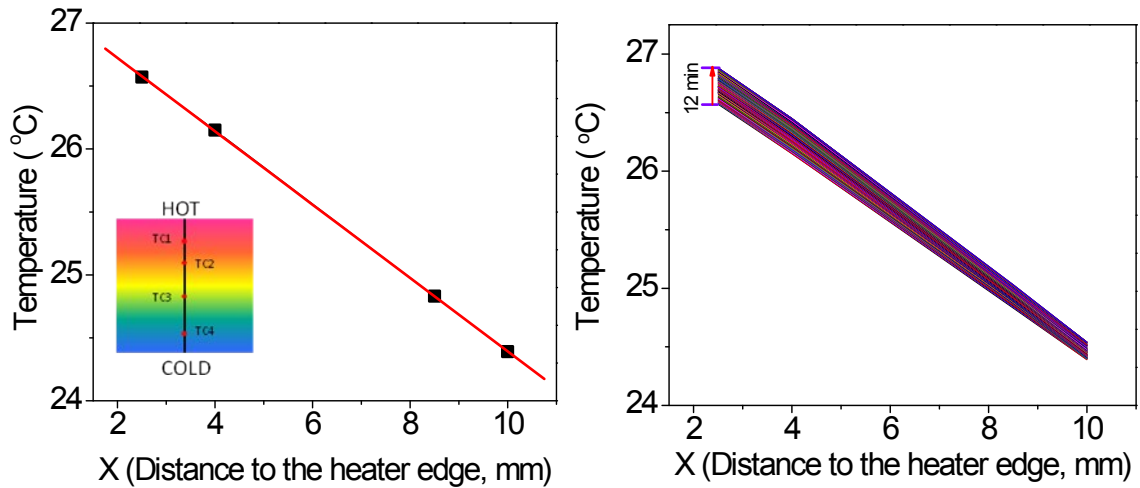
15

Figure S7. Linear temperature distributions across the polymer thin film on glass substrate. **a,** The measured temperature distribution in a line vertical to the heating direction with respect to the distance between the location where the temperature was measured and the heater edge as shown in the inset. **b,** The temperature distribution with respect to the distance between the location where the temperature was measured and the heater edge during 12 min heating time.
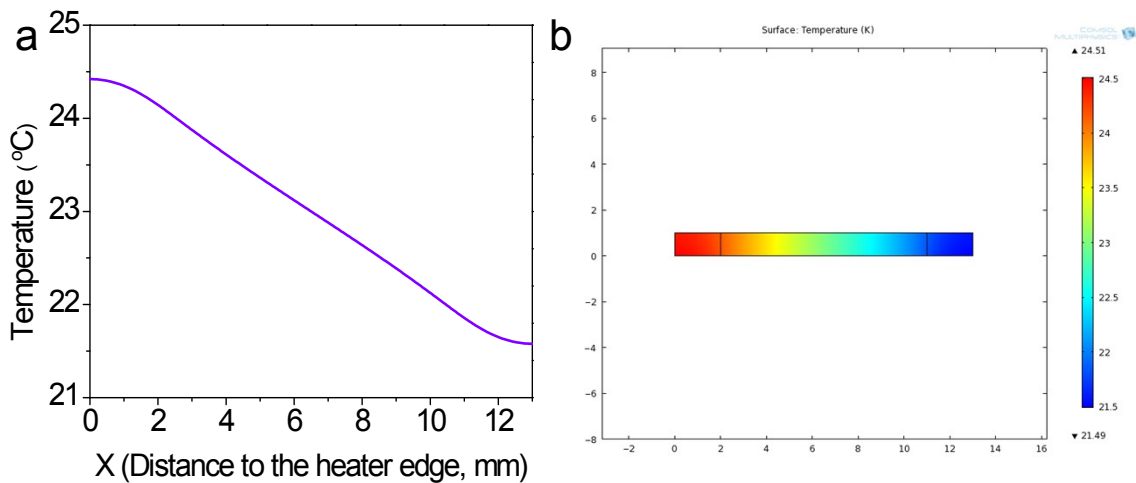

Figure S8. Simulated temperature distribution across thin film on glass substrate. **a,** The simulated temperature distribution in a line vertical to the heating direction with respect

to the distance between the location where the temperature was measured and the heater edge. **b,** The side-view of the simulated temperature profile.

Table S3. Measured Seebeck coefficients of selected samples with (S_1) or without (S_0) the addition of 0.2 wt% PEDOT NWs under the same EG treatment time.

Samples	S_0 (μV/K)	S_1 (μV/K)
5 vol% DMSO/PEDOT:PSS, EG 0 min	13.6±3.3	22.8±2.0
5 vol% DMSO/PEDOT:PSS, EG 50 min	23.4±5.1	35.8±2.2
5 vol% DMSO/PEDOT:PSS, EG 120 min	22.2±1.8	38.9±1.0
5 vol% DMSO/PEDOT:PSS, EG 220 min	25.6±5.2	37.2±4.3
5 vol% DMSO/PEDOT:PSS, EG 300 min	25.6±2.3	35.4±3.6
PEDOT-Tos	46.7±3.5	55.6±3.0

Note: The Seebeck coefficient ratio S_1/S_0 is defined as the ratio of Seebeck coefficient of the PEDOT:PSS matrix with (S_1) and without (S_0) the addition of PEDOT NWs under the same EG treatment time.

Table S4. Measured electrical conductivity, carrier mobility and calculated carrier concentration of PEDOT:PSS matrices without PEDOT NWs, and PEDOT:Tos matrix.

Samples	Electrical conductivity (S/cm)	Carrier mobility (cm^2/V.s)	Carrier concentration (cm^{-3})
5 vol% DMSO/PEDOT:PSS, EG 0 min	645.7±14.9	2.02±0.11	2.00×10^{21}
5 vol% DMSO/PEDOT:PSS, EG 50 min	762.6±34.1	2.41±0.26	1.98×10^{21}
5 vol% DMSO/PEDOT:PSS, EG 120 min	934.4±47.8	3.18±0.35	1.83×10^{21}
5 vol% DMSO/PEDOT:PSS, EG 220 min	629.8±22.1	3.51±0.18	1.12×10^{21}
PEDOT-Tos	1472.5±59.4	1.78±0.13	5.16×10^{21}

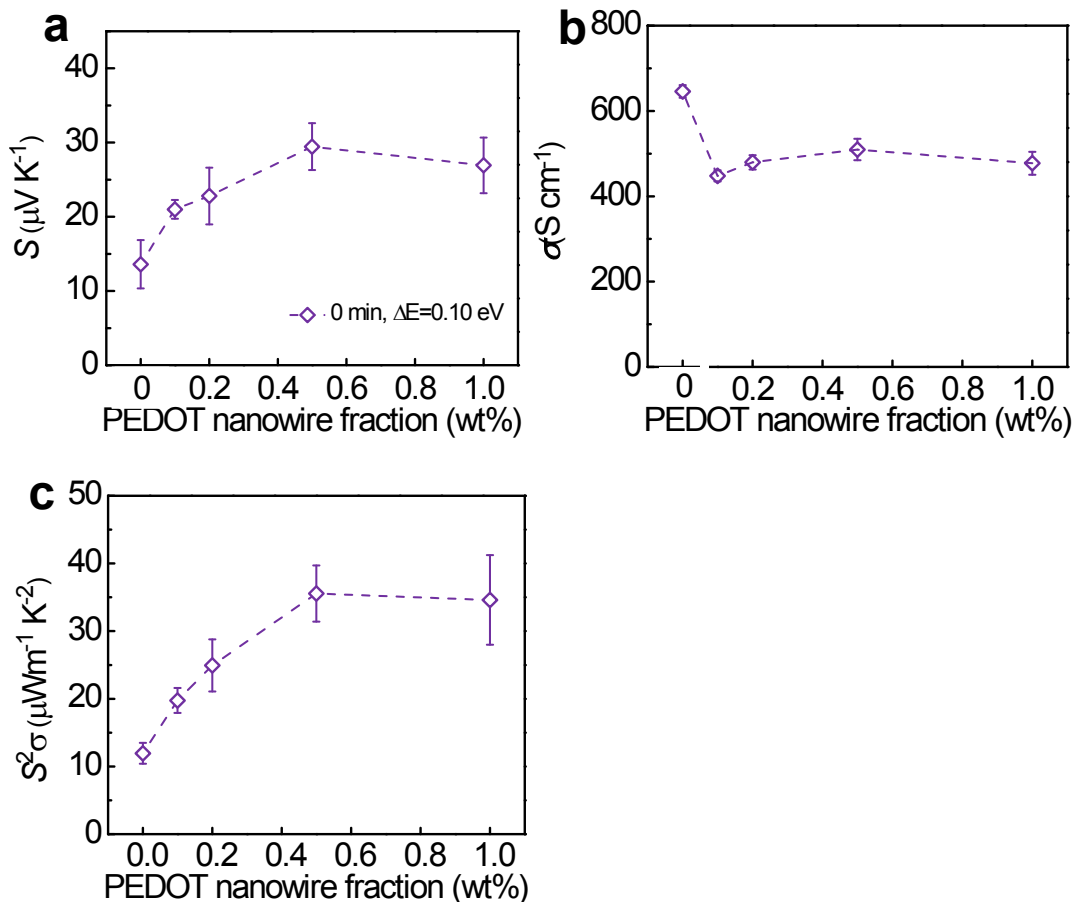*Note: EG-treated PEDOT:PSS was mixed with 5 vol% DMSO before treatments.*

Figure S9. Thermoelectric properties of PEDOT NWs/PEDOT:PSS hybrids without EG treatments. **a,** Seebeck coefficient. **b,** Electrical conductivity. **c,** Power factor *PF* of PEDOT:PSS hybrids. Note: PEDOT:PSS was mixed with 5 vol% DMSO before treatments.

6. Thermal conductivity measurements

6.1 Specific heat measurements

The specific heat of polymers was calculated using DSC spectra performed with METTLER TOLEDO thermal analysis system with the measurement error of 3.7 %. 40 μl aluminum crucibles were chosen as reference, blank and sample crucibles for good

thermal contact between samples and the bottom of crucible. The reference crucible was maintained in the same position for all measurements. Different PEDOT:PSS composites were prepared and dried in the same condition as that for thermoelectric property measurements . The composites were cold-pressed into small pellets for better thermal contact with the crucible bottom. The sample weight ranging from 4 to 7 mg was loaded for higher accurate measurements. The temperature ranges from 0 to 60 ℃ with an initial isothermal stage at 0 ℃ for 3 min, then the sample was heated up with the heat rate of 10 ℃ /min from 0 ℃ to 60 ℃. By recording the heat flow rate as a function of temperature and subtracting the heat flow rate for the blank crucible (blank curve) under the same condition, the specific heat at room temperature is determined using the formula $C_p=HF/m\beta$, where HF is the heat flow rate for the measured sample, m is the mass of the sample (mg), and β is the heating rate (℃ /min).

6.2 Thermal diffusivity measurements

It is challenging to measure the thermal diffusivity of nanoscaled-thick polymer films, thick polymer films (~20 μm) were prepared by drop-casting polymer solution on aluminum alloy 6061-T6 (1.5 mm thick) and treated in the same condition as that for thermoelectric property measurements. Laser flash technique was applied to measure the thermal diffusivity of PEDOT nanowire/PEDOT:PSS composites. The thermal diffusivity measurement was performed by using a two-layer method with Netzsch LFA 447 with a theoretical error of ~10%.[17]
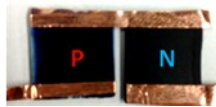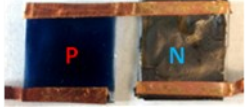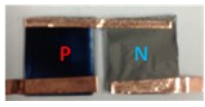
The film density $\rho=m/V$ was determined by measuring the film volume V (thickness × length ×width) and mass m. The thickness was measured by SEM (Hitachi 4300, 10 kV).

Finally, the thermal conductivity is calculated by $\kappa=\rho\alpha Cp$, where ρ is the density (g cm^{-3}), α is the thermal diffusivity (mm^2 s^{-1}), and C_p is the specific heat (J g^{-1} K^{-1}).

7. Thermoelectric power output measurements of OTEGs

The power output performance of assembled OTEGs based on the optimized organic hybrids was investigated with different types of *n*-type organic materials. The optimized organic hybrid films were assembled with Nitrogen-doped graphene based composite films using adhesive copper foils (3M Inc) as interconnects. (Table S5) The assembled OTEGs have their maximum power output as defined by $P_{max}=U^2/4R_I$ (where, P_{max} is the maximum power output, U is the measured Seebeck voltage, and R_I is the inner resistance of OTEG).[18] The temperature difference was created by one Peltier cooler and one Peltier heater, and was measured by two T-type thermocouples. The Seebeck voltage was measured by Keithley 2182A nanovoltmeter.

Table S5. Geometry details of OTEG devices

	OTEG1		OTEG2		OTEG3		OTEG4	
	P-leg	*N*-leg	*P*-leg	*N*-leg	*P*-leg	*N*-leg	*P*-leg	*N*-leg
Thickness (μm)	2.65	14.38	2.65	8.86	2.65	8.86	0.20	8.86
Lateral dimension (mm×mm)	13×13	13×13	13×13	13×13	13×13	13×13	13×13	13×13
Photo image								

Note: OTEG1 consists of N-doped graphene/PEI thin film (54/1(w/w), *n*-type leg) and nominal 0.2 wt% PEDOT NWs/PEDOT:PSS thin film (*p*-type leg); OTEG2 consists of BBL immersed N-doped graphene film (*n*-type leg) and nominal 0.2 wt% PEDOT NWs/PEDOT:PSS thin film (*p*-type leg); OTEG3 consists of N-doped graphene freestanding film (*n*-type leg) and nominal 0.2 wt% PEDOT NWs/PEDOT:PSS thin film (*p*-type leg); OTEG4 consists of N-doped graphene

freestanding film (*n*-type leg) and nominal 0.2 wt% PEDOT NWs/PEDOT:Tos thin film (*p*-type leg).

Supporting references

[1] M. G. Han, S. H. Foulger, *Small* **2006**, 2, 1164.

[2] P. Hojati-Talemi, C. Bächler, M. Fabretto, P. Murphy, D. Evans, *ACS Appl. Mater. Interfaces* **2013**, 5, 11654.

[3] O. Bubnova, Z. U. Khan, H. Wang, S. Braun, D. R. Evans, M. Fabretto,P. Hojati-Talemi, D. Dagnelund, J.-B. Arlin, Y. H. Geerts, S. Desbief,D. W. Breiby, J. W. Andreasen, R. Lazzaroni, W. M. Chen, I. Zozoulenko,M. Fahlman, P. J. Murphy, M. Berggren, X. Crispin, *Nat. Mater.* **2014**, 13, 190.

[4]. Li, J.; Ma, P. C.; Chow, W. S.; To, C. K.; Tang, B. Z.; Kim, J.-K, *Adv. Funct. Mater.* **2007**, 17, 3207.

[5]. Chandrasekhar, S. *Liquid crystals*, Cambridge University Press, New York **1992**, Chapter 2.

[7] Q. Wei, M. Mukaida, Y. Naitoh, T. Ishida, *Adv. Mater.* **2013**, 25, 2831.

[8] N. Massonnet, A. Carella, A. Geyer, J. Faure-Vincent, J. –P. Simonato, *Chem. Sci.* **2015**, 6, 412.

[8] J. Lee, M. J. Panzer, Y. He, T. P. Lodge, C. D. Frisbie, *J. Am. Chem. Soc.*, 2007, 129 (15), 4532.

[9] J. Lee, L. G. Kaake, J. H. Cho, X.-Y. Zhu, T. P. Lodge, C. D. Frisbie, *J. Phys. Chem. C*, 2009, 113 (20), 8972.

[10] O. Larsson, A. Laiho, W. Schmickler, M. Berggren, X. Crispin . *Adv. Mater.* **2011**, *23*, 4764.

[11] J. D. Yuen, A. S. Dhoot, E. B.Namdas, N. E. Coates, M. Heeney, I. McCulloch, D. Moses, A. J. Heeger, *J. Am. Chem. Soc.*, **2007**, 129(46), 14367.

[12] A. Laihoa, L. Herlogssona, R. Forchheimerb, X. Crispina, M. Berggren, *Proc. Natl. Acad. Sci. USA* **2011**, 108(37), 15069.

[13] C. L. Perkins, F. S. Hasoon, *J. Vac. Sci. Technol. A* **2006**, 24, 497.

[14] E. E. Haller, Semiconductor materials, Lecture notes for MSE 223, Department of Materials Science and Engineering, University of California Berkely.

[15] S. v. Reenen, M. Kemerink, *Org. Electron*. **2014**, 15, 2250.

[16] Zhang, K.; Wang, S.; Zhang, X.; Zhang, Y.; Cui, Y.; Qiu, J. *Nano Energy* **2015**, 13, 327-335.

[17] Campbell, R. C. Approximations in the use of two and three layer analysis models in flash diffusivity measurements. *Thermal Conductivity 30/Thermal Expansion 18* DEStech Publication Inc, Lancaster, (2010).

[18] Bubnova, O.; Khan, Z. U.; Malti, A.; Braun, S.; Fahlman, M.; Berggren, M.; Crispin, X. *Nat. Mater.* **2011**, 10, 429-433.